

Quantum Simulation of Hyperbolic Space with Circuit Quantum Electrodynamics: From Graphs to Geometry

Igor Boettcher,^{1,*} Przemyslaw Bienias,^{1,2} Ron Belyansky,¹ Alicia J. Kollár,¹ and Alexey V. Gorshkov^{1,2}

¹*Joint Quantum Institute, University of Maryland, College Park, MD 20742, USA*

²*Joint Center for Quantum Information and Computer Science,
NIST/University of Maryland, College Park, Maryland 20742, USA*

We show how quantum many-body systems on hyperbolic lattices with nearest-neighbor hopping and local interactions can be mapped onto quantum field theories in continuous negatively curved space. The underlying lattices have recently been realized experimentally with superconducting resonators and therefore allow for a table-top quantum simulation of quantum physics in curved background. Our mapping provides a computational tool to determine observables of the discrete system even for large lattices, where exact diagonalization fails. As an application and proof of principle we quantitatively reproduce the ground state energy, spectral gap, and correlation functions of the noninteracting lattice system by means of analytic formulas on the Poincaré disk, and show how conformal symmetry emerges for large lattices. This sets the stage for studying interactions and disorder on hyperbolic graphs in the future. Our analysis also reveals in which sense discrete hyperbolic lattices emulate the continuous geometry of negatively curved space and thus can be used to resolve fundamental open problems at the interface of interacting many-body systems, quantum field theory in curved space, and quantum gravity.

Quantum field theory and the theory of general relativity are main pillars of our quantitative description of nature. The current lack of a unified theory combining both, however, hinders us from addressing important questions related to early cosmology, black hole physics, and the quantum nature of spacetime [1, 2]. Furthermore, many recent theoretical developments in the context of holography and quantum information point towards a deep connection between geometry, entanglement, and renormalization [3–8]. To advance our understanding of quantum physics in curved space, it is crucial to create experimental setups for exploring the underlying effects in a tunable manner.

Important progress towards the quantum simulation of curved space has been made in nonlinear optical media [9–15], ultracold quantum gases [16–20], and other platforms [21–25], which allowed, for instance, for observation of event horizons [26, 27] and Hawking radiation [28, 29]. In these experiments, curvature is often emulated in Euclidean geometries through nonlinear field propagation. A complementary path was followed in recent cutting-edge experiments in circuit quantum electrodynamics (QED) [30–34], where hyperbolic geometry was emulated directly through photon dynamics confined to a hyperbolic lattice made from superconducting resonators [35, 36]. The setup is highly tunable and can be used to achieve photon interactions, coupling to spin degrees of freedom, or the effects of disorder [37–39]. Hyperbolic lattices have been investigated in the context of classical [40–45] and quantum spin systems [46], complex networks [47], and recently came into focus due to potential applications for fault-tolerant quantum codes [48–50].

In this Letter, we show that quantum many-body Hamiltonians relevant for circuit QED on hyperbolic lat-

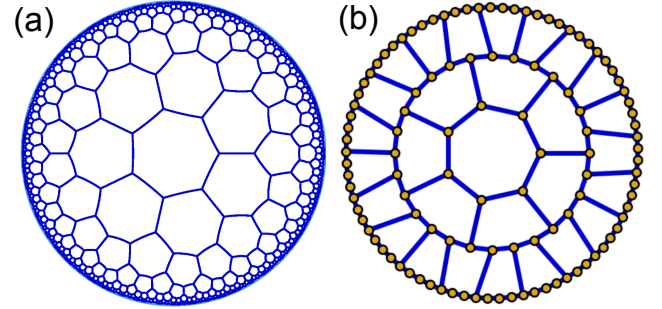


FIG. 1. (a) We consider the regular tessellation of the hyperbolic plane with heptagons, embedded into the Poincaré disk with a hyperbolic metric. All neighboring lattice sites have equal hyperbolic distance and the unit disk boundary is infinitely far away from each point in the interior. (b) Finite graphs preserving sevenfold rotation invariance can be constructed by considering subsets that are topologically equivalent to $\ell = 1, 2, 3 \dots$ concentric rings, shown here for $\ell = 3$.

tices can be approximated by a continuum theory on the Poincaré disk. This provides a computational tool to access observables even for otherwise intractable very large lattices, and shows that the discrete setup constitutes a quantum simulation of continuous hyperbolic space. We provide a dictionary between discrete and continuous geometry. To show the strength of our mapping, we quantitatively reproduce the ground state energy, spectral gap, and correlation functions for the noninteracting theory by analytic continuum formulas. We reveal how conformal symmetry emerges on hyperbolic lattices, implying significant computational simplifications in applications.

The dynamics of the circuit QED experiments of Ref. [35] can be described by nearest-neighbor hopping on a hyperbolic graph G , see Fig. 1. We assume for concrete-

number of rings ℓ	1	2	3	4	5	6	7	8	9	10
number of graph sites N	7	35	112	315	847	2240	5887	15435	40432	105875
effective disk radius L	0.447	0.745	0.894	0.958	0.984	0.994	0.998	0.9990	0.9997	0.9999
ground state energy (graph) E_0	-2	-2.636	-2.787	-2.847	-2.877	-2.894	-2.905	-2.91	-2.92	-2.92
ground state energy (continuum) $E_0^{(\text{cont})}$	-1.500	-2.570	-2.770	-2.842	-2.876	-2.895	-2.906	-2.914	-2.920	-2.924

TABLE I. The total number of sites $N = 7[(\frac{3+\sqrt{5}}{2})^\ell + (\frac{3-\sqrt{5}}{2})^\ell - 2]$ grows exponentially as a function of the number of rings ℓ . Each finite graph is mapped onto a continuous disk of radius $L = \sqrt{N/(N+28)}$. The ground state energy E_0 of the hopping Hamiltonian (1), defined as the lowest eigenvalue of the matrix $H = -A$, can be estimated from the lowest eigenvalue of Δ_g on the finite disk of radius $L < 1$, which gives $E_0^{(\text{cont})}$. Both values agree excellently for sufficiently large ℓ , see also Fig. 2. For $\ell \geq 8$ we have to resort to less precise sparse matrix methods to estimate E_0 [51].

ness that G is part of a planar hyperbolic tessellation with regular heptagons, $\{7, 3\}$ in Schläfli notation, but the results generalize to $\{p, 3\}$ with $p \geq 7$. The actual experiments realize the line graph of G [36], but their continuum approximation is analogous. Consider then the nearest-neighbor hopping Hamiltonian

$$\hat{\mathcal{H}}_0 = -t \sum_{i,j \in G} \hat{a}_i^\dagger A_{ij} \hat{a}_j, \quad (1)$$

with \hat{a}_i^\dagger the photon creation operator on site i and $t > 0$. The entry A_{ij} of the adjacency matrix A is 1 if sites i and j are connected by an edge, and zero otherwise [51]. We construct finite hyperbolic graphs that preserve sevenfold rotation invariance from $\ell = 1, 2, 3, \dots$ successive quasi-concentric rings, where $\ell = 1$ corresponds to a single heptagon, see Fig. 1. The total number of sites grows exponentially as $N \sim 7\varphi^{2\ell}$ for large ℓ , with $\varphi = (1 + \sqrt{5})/2$ the golden ratio [44, 45], see Table I. Sites in the interior of G have coordination number 3, and sites on the boundary have either 2 or 3. The average coordination number for large ℓ is $3 - 1/\sqrt{5} = 2.553$ and there is always a significant fraction of boundary sites.

We embed the hyperbolic lattice into the Poincaré disk $\mathbb{D} = \{z \in \mathbb{C}, |z| < 1\}$ with the hyperbolic metric

$$ds^2 = \frac{dx^2 + dy^2}{(1 - |z|^2)^2}. \quad (2)$$

(We write $z = x + iy = re^{i\phi}$.) Let us recall some properties of this space of constant negative curvature [52]: The hyperbolic distance between two points $z, z' \in \mathbb{D}$ is

$$d(z, z') = \frac{1}{2} \text{arcosh} \left(1 + \frac{2|z - z'|^2}{(1 - |z|^2)(1 - |z'|^2)} \right), \quad (3)$$

which reduces to $|z - z'|$ for $|z|, |z'| \ll 1$. The boundary of \mathbb{D} is infinitely far from every point in the interior and the area of a disk of radius $L < 1$ is $\pi L^2/(1 - L^2)$. The isometries (distance preserving maps) of \mathbb{D} are given by conformal automorphisms

$$z \mapsto w(z) = e^{i\eta} \frac{a - z}{1 - z\bar{a}} \quad (4)$$

with $\eta \in [0, 2\pi)$ and $a \in \mathbb{D}$. These transformations exchange a with the origin, and so each point in \mathbb{D} is equivalent. The group of mappings (4) is isomorphic to the group $\text{PSL}(2, \mathbb{R})$ of Möbius transformations on the upper half-plane.

We now assign a coordinate $z_i \in \mathbb{D}$ to each site $i \in G$ so that neighboring sites are separated by a uniquely specified hyperbolic distance $d_0 = 0.283128$ [51, 53]. Every function $f : \mathbb{D} \rightarrow \mathbb{C}$ induces a function on the graph via $i \mapsto f(z_i)$. On the Euclidean square lattice, nearest-neighbor hopping Hamiltonians of type (1) are related to the Laplacian through a finite difference approximation, facilitating powerful techniques such as the continuum theory of solids or lattice gauge theory in high-energy physics. Our goal is to approximate the adjacency matrix on the heptagonal lattice by the *hyperbolic Laplacian*

$$\Delta_g = (1 - |z|^2)^2 (\partial_x^2 + \partial_y^2). \quad (5)$$

This is the Laplace–Beltrami operator associated to the hyperbolic metric on the Poincaré disk and it is invariant under conformal automorphisms [52, 54, 55].

Consider a lattice site z_i with coordination number 3 and a sufficiently smooth function $f : \mathbb{D} \rightarrow \mathbb{C}$. We have $A_{ij}f(z_j) = f(z_{i+e_1}) + f(z_{i+e_2}) + f(z_{i+e_3})$, where the right hand side represents the sum over the neighbors of z_i and we implicitly sum over repeated indices. To manipulate this expression, apply an automorphism $z \mapsto w(z)$ from Eq. (4) with $\eta = 0$ and $a = z_i$. This exchanges z_i with the origin. Furthermore, the three neighbors of z_i are mapped to form an equilateral triangle with coordinates $w_1 = he^{i\chi_i}$, $w_2 = he^{i\chi_i}e^{i2\pi/3}$, $w_3 = he^{i\chi_i}e^{i4\pi/3}$, and $h = \tanh(d_0) = 0.275798$. The phase χ_i depends on the coordinate z_i in a nontrivial manner [51]. Applying the inverse automorphism we arrive at the identity

$$A_{ij}f(z_j) = f\left(\frac{z_i - w_1}{1 - w_1\bar{z}_i}\right) + f\left(\frac{z_i - w_2}{1 - w_2\bar{z}_i}\right) + f\left(\frac{z_i - w_3}{1 - w_3\bar{z}_i}\right). \quad (6)$$

This equation can be expanded in powers of h , with the linear term vanishing due to $w_1 + w_2 + w_3 = 0$, and the

quadratic term being universal and independent of χ_i :

$$A_{ij}f(z_j) = 3f(z_i) + \frac{3}{4}h^2\Delta_g f(z_i) + \mathcal{O}(h^3). \quad (7)$$

This relation between adjacency matrix and hyperbolic Laplacian constitutes the first main result of this work. The $\mathcal{O}(h^3)$ -correction and the modification for boundary sites with coordination number 2 are discussed in the supplemental material (SM) [51].

Our second main result towards a continuum theory for hyperbolic lattices is a formula to approximate sums over lattice sites by integrals over the Poincaré disk. For suitable functions $f: \mathbb{D} \rightarrow \mathbb{C}$ we have

$$\sum_{i \in G} f(z_i) \approx \frac{28}{\pi} \int_{|z| \leq L} \frac{d^2 z}{(1 - |z|^2)^2} f(z), \quad (8)$$

where $d^2 z / (1 - |z|^2)^2$ is the infinitesimal hyperbolic volume element. Importantly this implies that a finite graph with ℓ rings and $N(\ell)$ sites corresponds to a finite continuous disk with effective radius

$$L = \sqrt{\frac{N}{N + 28}}. \quad (9)$$

We display the first ten radii in Table I. The path to show Eq. (8) is as follows [51]. The discrete phases of coordinates $z_i = r_i e^{i\phi_i}$ are almost uniformly distributed, and so we may replace them by a continuous variable $\phi \in [0, 2\pi)$ and the sum by a Riemann integral. After angular integration we arrive at a sum of the type $\sum_i f(r_i)$, which can be approximated by $\int_{r \leq L} dN f(r)$ with $N(r) = \sum_i \Theta(r - r_i)$ and Θ the Heaviside step function. Introducing the hyperbolic invariant $\rho = \frac{1+r^2}{1-r^2}$ we numerically find $N(r) \approx C\rho + C'$ with $C = 14$. Using $dN = C d\rho = 4C \frac{dr}{(1-r^2)^2}$ we eventually arrive at Eq. (8). The effective radius L is determined such that the right hand side of Eq. (8) yields N when inserting $f = 1$. Although the parameter C is fitted empirically, changing its value would merely require to replace $28 \rightarrow 2C$ in Eqs. (8) and (9).

These results make it possible to approximate A_{ij} and $\sum_{i \in G}$ in the bulk of the graph by their continuum counterparts. As an example consider the Bose–Hubbard model Hamiltonian on the hyperbolic lattice

$$\hat{\mathcal{H}} = \sum_{i \in G} \left[-t \sum_{j \in G} \hat{a}_i^\dagger A_{ij} \hat{a}_j - \mu \hat{a}_i^\dagger \hat{a}_i + U(\hat{a}_i^\dagger \hat{a}_i)^2 \right], \quad (10)$$

with chemical potential μ and on-site interaction U . The corresponding continuum Hamiltonian is

$$\hat{\mathcal{H}}' = \int_{|z| \leq L} \frac{d^2 z}{(1 - |z|^2)^2} \left[\hat{\alpha}_z^\dagger (-J\Delta_g - \mu') \hat{\alpha}_z + U'(\hat{\alpha}_z^\dagger \hat{\alpha}_z)^2 \right] \quad (11)$$

with $J = \frac{3}{4}h^2 t$, $\mu' = \mu + 3t$, $U' = \frac{\pi}{28}U$. The field operators $\hat{\alpha}_z = \hat{\alpha}(z)$ satisfy $[\hat{\alpha}(z), \hat{\alpha}^\dagger(z')] = (1 - |z|^2)^2 \delta^{(2)}(z -$

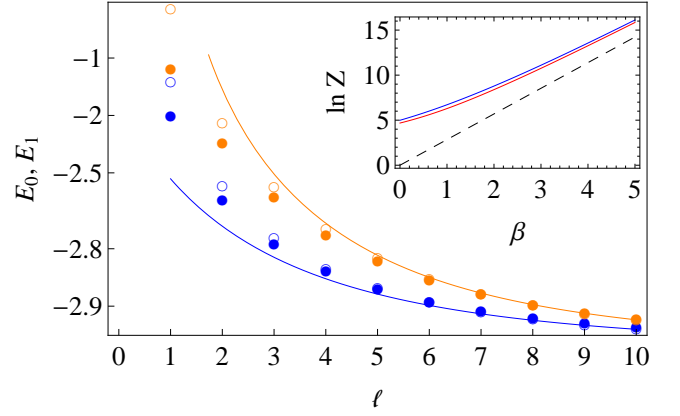


FIG. 2. Ground state energy E_0 (blue, lower data) and first excited state energy E_1 (orange, upper data) for the graph (filled circles) and corresponding continuous disk (empty circles). The solid lines are the asymptotic continuum formulas from Eq. (14). Inset: Partition function Z summed over negative energies for the graph with $\ell = 4$ (blue) and associated disk (red) as a function of inverse temperature β . The dashed line is the low-temperature asymptote $\ln Z \sim -\beta E_0$.

$z')$ and $\hat{\alpha}(z_i) = \sqrt{28/\pi} \hat{a}_i$. We deliberately ignore boundary effects, although holographic models [56–58] are a fascinating application that we leave for future work.

The spectral theory of the hyperbolic Laplacian on the Poincaré disk is well-understood [51, 54, 55]. The eigenvalues of $-\Delta_g$ are

$$\varepsilon = 1 + k^2 \quad (12)$$

with $k \geq 0$. The corresponding eigenfunctions in radial coordinates are $\psi_{km}(r) e^{im\phi}$ with $m \in \mathbb{Z}$ and

$$\psi_{km}(r) = P_{\frac{1}{2}(-1+ik)}^m \left(\frac{1+r^2}{1-r^2} \right), \quad (13)$$

where P_ν^m is the Legendre function of the first kind. Restricting space to a finite disk of radius $L < 1$ and imposing Dirichlet boundary conditions, $\psi_{km}(L) = 0$, yields a discrete spectrum $\varepsilon_n = 1 + k_n^2$ with $k_n > 0$.

As a first application of the continuum theory, we estimate ground state energy and spectral gap of the Hamiltonian in Eq. (1). We set $t = 1$. Since $\hat{\mathcal{H}}_0$ is quadratic this reduces to determining the lowest two eigenvalues of the matrix $H = -A$, which we label E_0 and $E_1 = E_0 + \delta E$ with spectral gap $\delta E > 0$. Note that the spectrum of H is contained in the real interval $(-3, 3)$. For infinite lattices the ground state energy is strictly limited [36, 59, 60] by $\lim_{\ell \rightarrow \infty} E_0 \in [-2.966, -2.862]$. We approximate H by the differential operator $H^{(\text{cont})} = -3 - \frac{3}{4}h^2\Delta_g$ on the disk of radius $L = \sqrt{N/(N+28)}$. Its eigenvalues are $E_n^{(\text{cont})} = -3 + \frac{3}{4}h^2(1 + k_n^2)$. As $\ell \rightarrow \infty$, the lowest possible $k_n \rightarrow 0$, which yields the ground state energy $\lim_{\ell \rightarrow \infty} E_0^{(\text{cont})} = E_\infty = -3 + \frac{3}{4}h^2 = -2.94295$, consistent with the graph bound. For finite $\ell \geq 1$, the

first two eigenvalues of $H^{(\text{cont})}$ are readily computed from $\psi_{km}(L) = 0$ for $m = 0, 1$, respectively, and agree remarkably well with the graph data for $\ell \gtrsim 4$, see Table I and Fig. 2. For $\ell \rightarrow \infty$ we have [51]

$$E_{0,1}^{(\text{cont})} \sim E_\infty + \frac{3\pi^2 h^2}{4} \frac{1}{(\ln \varphi \cdot \ell + c_{0,1})^2}, \quad (14)$$

with $\varphi = (1 + \sqrt{5})/2$, $c_0 = \ln 2$, and $c_1 = \ln 2 - 1$.

As we go to higher energies, the spectra of H and $H^{(\text{cont})}$ start to deviate more and more. Still, the graph and continuum partition functions $Z = \sum_n \Theta(-E_n) e^{-\beta E_n}$ and $Z' = \sum_n \Theta(-E_n^{(\text{cont})}) e^{-\beta E_n^{(\text{cont})}}$ with inverse temperature β agree well, see the inset of Fig. 2. (We limit the sums to negative energies to roughly cut off high energy contributions clearly outside the continuum approximation.) The ability to *quantitatively* reproduce the low-energy graph spectrum and predict the behavior for large graphs by means of the continuum approximation constitutes the third main result of this work.

Our second application of the continuum theory is the computation of correlation functions on the graph from the continuum Green function. We denote the Green function of $H = -A$ by

$$G_{ij}(\omega) = \left(\frac{1}{H - \omega} \right)_{ij} = \sum_{n=1}^N \frac{\psi_n(i) \psi_n^*(j)}{E_n - \omega}. \quad (15)$$

Here ψ_n and E_n are the eigenvectors and eigenenergies of H , $H\psi_n = E_n\psi_n$, and $\omega \in \mathbb{C}$ is a complex frequency. $G_{ij}(\omega)$ constitutes the measurable two-point correlation function $\langle \hat{a}_i(\omega) \hat{a}_j^\dagger(\omega) \rangle_0$ for the free theory averaged with respect to \hat{H}_0 , and can be written as an auxiliary field Gaussian path integral on the graph. Approximating the latter by the continuum expressions we obtain [51]

$$G_{ij}(\omega) \approx \frac{\pi}{21h^2} G\left(z_i, z_j, \frac{4(\omega + 3)}{3h^2}, L\right). \quad (16)$$

Here $G(z, z', \lambda, L)$ is the Green function of the hyperbolic Helmholtz operator, satisfying $(\lambda + \Delta_g)G(z, z', \lambda, L) = -(1 - |z|^2)^2 \delta^{(2)}(z - z')$ and Dirichlet boundary conditions $G(z, z', \lambda, L) = 0$ for $|z| = L$ or $|z'| = L$. Again, the disk radius L is matched to ℓ through Eq. (9). The accuracy of the approximation in Eq. (16) is remarkably good as we show in Fig. 3.

The continuum Green function $G(z, z', \lambda, L)$ is uniquely specified by the Dirichlet boundary condition [55, 61–63]. The full but lengthy analytic expression is given in the SM [51]. As $L \rightarrow 1$, it is solely a function of the hyperbolic distance $d(z, z')$ due to automorphism invariance. For example, for $\lambda = 0$ we have

$$G(z, z', 0, L) = -\frac{1}{4\pi} \ln \left| \frac{L(z - z')}{L^2 - zz'} \right|^2, \quad (17)$$

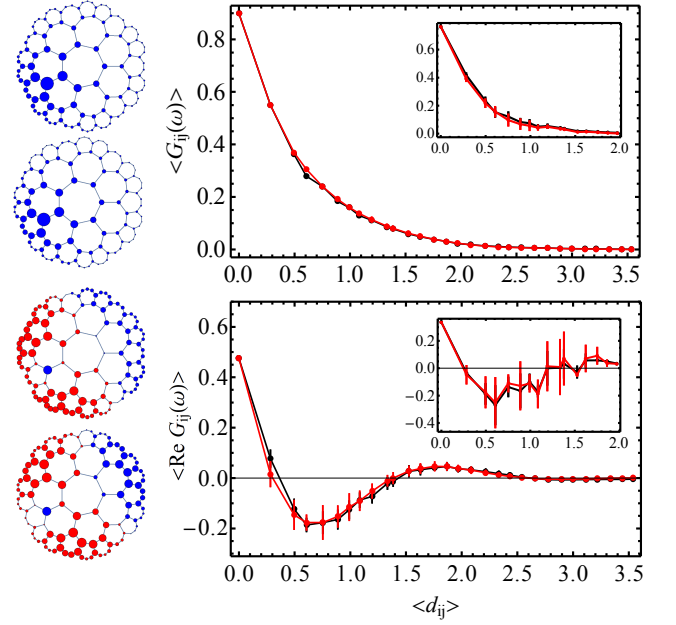


FIG. 3. Quantitative match between graph Green function G_{ij} and continuum Green function $G(z_i, z_j)$. We fix site z_i to be on the 2nd ring, and plot the correlations as a function F_j of site z_j . *Upper panel.* Results for $\omega = -2.95$ just below E_0 . (*Left*). The two plots are $F_j = G_{ij}$ and $F_j = G(z_i, z_j)$. The size of dots is proportional to $|F_j|^{1/2}$, and blue/red corresponds to positive/negative sign of F_j . (*Right*). Mean correlation function vs. hyperbolic distance $d_{ij} = d(z_i, z_j)$, where the red (black) data is the graph (continuum) function. To obtain the curves, we make a list of pairs (F_j, d_{ij}) and compute the average F_j as a function of distance, with the error bar being the standard deviation. The quantitative agreement between graph and continuum is remarkable. Emergent conformal symmetry is reflected by the data points collapsing onto a single curve $G_{ij} = f(d_{ij})$ with some function f for large ℓ . The main plots are for $\ell = 6$, the insets for $\ell = 3$. *Lower panel.* The same setting for $\omega = -2.5 + 0.1i$ with $\text{Re}(\omega) > E_0$. We plot the real part of the correlation function.

which is a function of $\tanh d(z, z') = \left| \frac{z - z'}{1 - \bar{z}z'} \right|$ for $L = 1$. In turn, this implies that also the graph correlation function $G_{ij}(\omega)$ is approximately a universal function of the hyperbolic distance $d_{ij} = d(z_i, z_j)$ for large ℓ , as is shown in Fig. 3. The *quantitative* matching of graph and continuum Green functions and the finding of emergent conformal symmetry on the hyperbolic lattice constitute our fourth main result of this work.

The continuum approximation for hyperbolic lattices that we have put forward provides a computational framework to efficiently compute observables relevant for future circuit QED experiments simulating curved spaces: the continuum Green functions can be used in diagrammatic techniques to explore interactions between photons and other degrees of freedom such as qubits by means of Fourier analysis on hyperbolic space. The strong coupling regime in experiment then constitutes an

important benchmark for our theoretical description of nonperturbative quantum physics in curved space. The continuum formalism naturally connects to statements of AdS/CFT correspondence and the intriguing interplay between the boundary field theory and the hyperbolic bulk. Disorder on very large lattices can also be studied with the continuum approximation. Time-dependent phenomena such as the spreading of local information or nonequilibrium time evolution of quantum fields is encapsulated in the continuum theory and can be measured with transmission experiments.

Acknowledgments. We gratefully acknowledge collaboration and many inspiring discussions with R. Lundgren and A. Houck. We thank T. Jacobsen, V. Galitski, B. Swingle, and Y. Wang for insightful comments. This work was supported by DoE BES QIS program (award No. DESC0019449), ARO MURI, DoE ASCR Quantum Testbed Pathfinder program (award No. DESC0019040), DoE ASCR FAR-QC (award No. DE-SC0020312), NSF PFCQC program, AFOSR, ARL CDQI, and NSF PFC at JQI. R. B. acknowledges support from NSERC and FRQNT.

* iboettch@umd.edu

- [1] L. Parker and D. Toms, *Quantum Field Theory in Curved Spacetime: Quantized Fields and Gravity* (Cambridge University Press, Cambridge, 2009).
- [2] D. Oriti, ed., *Approaches to quantum gravity: Toward a new understanding of space, time and matter* (Cambridge University Press, Cambridge, 2009).
- [3] S. Ryu and T. Takayanagi, “Holographic Derivation of Entanglement Entropy from the anti-de Sitter Space/Conformal Field Theory Correspondence,” *Phys. Rev. Lett.* **96**, 181602 (2006).
- [4] G. Vidal, “Entanglement Renormalization,” *Phys. Rev. Lett.* **99**, 220405 (2007).
- [5] G. Vidal, “Class of Quantum Many-Body States That Can Be Efficiently Simulated,” *Phys. Rev. Lett.* **101**, 110501 (2008).
- [6] B. Swingle, “Entanglement renormalization and holography,” *Phys. Rev. D* **86**, 065007 (2012).
- [7] J. Haegeman, T. J. Osborne, H. Verschelde, and F. Verstraete, “Entanglement Renormalization for Quantum Fields in Real Space,” *Phys. Rev. Lett.* **110**, 100402 (2013).
- [8] A. Milsted and G. Vidal, “Geometric interpretation of the multi-scale entanglement renormalization ansatz,” (2018), arXiv:1812.00529.
- [9] U. Leonhardt and P. Piwnicki, “Relativistic Effects of Light in Moving Media with Extremely Low Group Velocity,” *Phys. Rev. Lett.* **84**, 822 (2000).
- [10] S. Batz and U. Peschel, “Linear and nonlinear optics in curved space,” *Phys. Rev. A* **78**, 043821 (2008).
- [11] D. A. Genov, S. Zhang, and X. Zhang, “Mimicking celestial mechanics in metamaterials,” *Nat. Phys.* **5**, 687 (2009).
- [12] I. I. Smolyaninov and E. E. Narimanov, “Metric Signature Transitions in Optical Metamaterials,” *Phys. Rev. Lett.* **105**, 067402 (2010).
- [13] H. Chen, R.-X. Miao, and M. Li, “Transformation optics that mimics the system outside a Schwarzschild black hole,” *Opt. Express* **18**, 15183 (2010).
- [14] R. Bekenstein, R. Schley, M. Mutzafi, C. Rotschild, and M. Segev, “Optical simulations of gravitational effects in the Newton–Schrödinger system,” *Nat. Phys.* **11**, 872 (2015).
- [15] R. Bekenstein, Y. Kabessa, Y. Sharabi, O. Tal, N. Engheta, G. Eisenstein, A. J. Agranat, and M. Segev, “Control of light by curved space in nanophotonic structures,” *Nat. Photonics* **11**, 664 (2017).
- [16] L. J. Garay, J. R. Anglin, J. I. Cirac, and P. Zoller, “Sonic Analog of Gravitational Black Holes in Bose-Einstein Condensates,” *Phys. Rev. Lett.* **85**, 4643 (2000).
- [17] I. Carusotto, S. Fagnocchi, A. Recati, R. Balbinot, and A. Fabbri, “Numerical observation of Hawking radiation from acoustic black holes in atomic Bose–Einstein condensates,” *New J. Phys.* **10**, 103001 (2008).
- [18] F. Caravelli, A. Hamma, F. Markopoulou, and A. Riera, “Trapped surfaces and emergent curved space in the Bose-Hubbard model,” *Phys. Rev. D* **85**, 044046 (2012).
- [19] O. Boada, A. Celi, J. I. Latorre, and M. Lewenstein, “Dirac equation for cold atoms in artificial curved spacetimes,” *New J. Phys.* **13**, 035002 (2011).
- [20] A. Kosior, M. Lewenstein, and A. Celi, “Unruh effect for interacting particles with ultracold atoms,” *SciPost Phys.* **5** (2018), 10.21468/scipostphys.5.6.061.
- [21] R. Schützhold and W. G. Unruh, “Hawking Radiation in an Electromagnetic Waveguide?” *Phys. Rev. Lett.* **95**, 031301 (2005).
- [22] B. Horstmann, B. Reznik, S. Fagnocchi, and J. I. Cirac, “Hawking Radiation from an Acoustic Black Hole on an Ion Ring,” *Phys. Rev. Lett.* **104**, 250403 (2010).
- [23] S. Weinfurter, E. W. Tedford, M. C. J. Penrice, W. G. Unruh, and G. A. Lawrence, “Measurement of Stimulated Hawking Emission in an Analogue System,” *Phys. Rev. Lett.* **106**, 021302 (2011).
- [24] C. Sheng, H. Liu, Y. Wang, S. N. Zhu, and D. A. Genov, “Trapping light by mimicking gravitational lensing,” *Nat. Photonics* **7**, 902906 (2013).
- [25] Z. Tian, J. Jing, and A. Dragan, “Analog cosmological particle generation in a superconducting circuit,” *Phys. Rev. D* **95**, 125003 (2017).
- [26] O. Lahav, A. Itah, A. Blumkin, C. Gordon, S. Rinott, A. Zayats, and J. Steinhauer, “Realization of a Sonic Black Hole Analog in a Bose-Einstein Condensate,” *Phys. Rev. Lett.* **105**, 240401 (2010).
- [27] T. G. Philbin, C. Kuklewicz, S. Robertson, S. Hill, F. König, and U. Leonhardt, “Fiber-Optical Analog of the Event Horizon,” *Science* **319**, 1367 (2008).
- [28] J. Steinhauer, “Observation of quantum Hawking radiation and its entanglement in an analogue black hole,” *Nat. Phys.* **12**, 959965 (2016).
- [29] J. Hu, L. Feng, Z. Zhang, and C. Chin, “Quantum simulation of Unruh radiation,” *Nat. Phys.* **15**, 785789 (2019).
- [30] A. A. Houck, H. E. Türeci, and J. Koch, “On-chip quantum simulation with superconducting circuits,” *Nat. Phys.* **8**, 292 (2012).
- [31] D. L. Underwood, W. E. Shanks, J. Koch, and A. A. Houck, “Low-disorder microwave cavity lattices for quantum simulation with photons,” *Phys. Rev. A* **86**, 023837 (2012).

- [32] S. Schmidt and J. Koch, “Circuit QED lattices: towards quantum simulation with superconducting circuits,” *Ann. Phys.* **525**, 395 (2013).
- [33] M. Fitzpatrick, N. M. Sundaresan, A. C. Y. Li, J. Koch, and A. A. Houck, “Observation of a Dissipative Phase Transition in a One-Dimensional Circuit QED Lattice,” *Phys. Rev. X* **7**, 011016 (2017).
- [34] B. M. Anderson, R. Ma, C. Owens, D. I. Schuster, and J. Simon, “Engineering Topological Many-Body Materials in Microwave Cavity Arrays,” *Phys. Rev. X* **6**, 041043 (2016).
- [35] A. J. Kollár, M. Fitzpatrick, and A. A. Houck, “Hyperbolic lattices in circuit quantum electrodynamics,” *Nature* **571**, 45 (2019).
- [36] A. J. Kollár, M. Fitzpatrick, P. Sarnak, and A. A. Houck, “Line-Graph Lattices: Euclidean and Non-Euclidean Flat Bands, and Implementations in Circuit Quantum Electrodynamics,” (2019), arXiv:1902.02794.
- [37] S. Schmidt, D. Gerace, A. A. Houck, G. Blatter, and H. E. Türeci, “Nonequilibrium delocalization-localization transition of photons in circuit quantum electrodynamics,” *Phys. Rev. B* **82**, 100507 (2010).
- [38] J. Raftery, D. Sadri, S. Schmidt, H. E. Türeci, and A. A. Houck, “Observation of a Dissipation-Induced Classical to Quantum Transition,” *Phys. Rev. X* **4**, 031043 (2014).
- [39] Neereja M. Sundaresan, Rex Lundgren, Guanyu Zhu, Alexey V. Gorshkov, and Andrew A. Houck, “Interacting Qubit-Photon Bound States with Superconducting Circuits,” *Phys. Rev. X* **9**, 011021 (2019).
- [40] R. Rietman, B. Nienhuis, and J. Oitmaa, “The Ising model on hyperlattices,” *J. Phys. A Math. Gen.* **25**, 6577 (1992).
- [41] H. Shima and Y. i Sakaniwa, “Geometric effects on critical behaviours of the Ising model,” *J. Phys. A Math. Gen.* **39**, 4921 (2006).
- [42] S. K. Baek, S. D. Yi, and B. J. Kim, “Diffusion on a heptagonal lattice,” *Phys. Rev. E* **77**, 022104 (2008).
- [43] R. Krčmar, A. Gendiar, K. Ueda, and T. Nishino, “Ising model on a hyperbolic lattice studied by the corner transfer matrix renormalization group method,” *J. Phys. A Math. Theor.* **41**, 125001 (2008).
- [44] S. K. Baek, P. Minnhagen, and B. J. Kim, “Percolation on hyperbolic lattices,” *Phys. Rev. E* **79**, 011124 (2009).
- [45] H. Gu and R. M. Ziff, “Crossing on hyperbolic lattices,” *Phys. Rev. E* **85**, 051141 (2012).
- [46] M. Daniška and A. Gendiar, “Analysis of quantum spin models on hyperbolic lattices and Bethe lattice,” *J. Phys. A Math. Theor.* **49**, 145003 (2016).
- [47] D. Krioukov, F. Papadopoulos, M. Kitsak, A. Vahdat, and M. Boguñá, “Hyperbolic geometry of complex networks,” *Phys. Rev. E* **82**, 036106 (2010).
- [48] N. P. Breuckmann and B. M. Terhal, “Constructions and Noise Threshold of Hyperbolic Surface Codes,” *IEEE T. Inform. Theory* **62**, 37313744 (2016).
- [49] N. P. Breuckmann, C. Vuillot, E. Campbell, A. Krishna, and B. M. Terhal, “Hyperbolic and semi-hyperbolic surface codes for quantum storage,” *Quantum Sci. Technol.* **2**, 035007 (2017).
- [50] A. Lavasani, G. Zhu, and M. Barkeshli, “Universal logical gates with constant overhead: instantaneous Dehn twists for hyperbolic quantum codes,” *Quantum* **3**, 180 (2019).
- [51] See Supplemental Material for details on creating hyperbolic lattices, continuum limit of tight-binding Hamiltonian, spectral theory of hyperbolic Laplacian, and formulas for continuum Green function.
- [52] J. W. Cannon, W. J. Floyd, R. Kenyon, and W. R. Parry, “Hyperbolic Geometry,” in *Flavors of Geometry*, Vol. 31, edited by S. Levy (MSRI Publications, 1997) p. 59.
- [53] See Supplementary File coordinates.dat containing the coordinates for the sites of the inner six rings, listed as real and imaginary parts.
- [54] P. Sarnak, “Spectra of hyperbolic surfaces,” *Bull. Amer. Math. Soc* **40**, 441–478 (2003).
- [55] J. Marklof, “Selberg’s Trace Formula: An Introduction,” in *Hyperbolic geometry and applications in quantum chaos and cosmology*, Vol. 397, edited by J. Bolte and F. Steiner (Cambridge University Press, 2012) p. 83.
- [56] D. T. Son, “Toward an AdS/cold atoms correspondence: A geometric realization of the Schrödinger symmetry,” *Phys. Rev. D* **78**, 046003 (2008).
- [57] K. Balasubramanian and J. McGreevy, “Gravity Duals for Nonrelativistic Conformal Field Theories,” *Phys. Rev. Lett.* **101**, 061601 (2008).
- [58] L. Boyle, B. Dickens, and F. Flicker, “Conformal Quasicrystals and Holography,” (2018), arXiv:1805.02665.
- [59] W. L. Paschke, “Lower bound for the norm of a vertex-transitive graph,” *Math. Z.* **213**, 225 (1993).
- [60] Y. Higuchi and T. Shirai, “Isoperimetric Constants of (d, f) -Regular Planar Graphs,” *Interdiscip. Inform. Sci.* **9**, 221 (2003).
- [61] M. Abramowitz and I. A. Stegun, *Handbook of Mathematical Functions with Formulas, Graphs, and Mathematical Tables*, Applied Mathematics Series No. 55 (U. S. Government Printing Office, Washington, DC, 1964).
- [62] J. Zinn-Justin, *Quantum Field Theory and Critical Phenomena*, 4th ed. (Oxford University Press, Oxford, 2002).
- [63] I. Boettcher and M. Holzmann, “Quasi-long-range order in trapped two-dimensional Bose gases,” *Phys. Rev. A* **94**, 011602 (2016).

Supplemental Material

CONTENTS

References	5
S1. Embedding coordinates	7
S2. Derivation of Eq. (7) and corrections	7
S3. Derivation of Eqs. (8) and (9)	9
S5. Eigenfunctions of hyperbolic Laplacian	10
S6. Computation of lowest eigenvalues and derivation of Eq. (14)	11
S4. Derivation of Eq. (16)	12
S7. Continuum Green function (Computation)	13
S8. Continuum Green function (Summary)	15

This supplemental material contains more detailed derivations of some equations of the main text. Further, the eigenfunctions of the hyperbolic Laplacian are summarized and we present a complete computation of the continuum Green function with Dirichlet boundary conditions. Readers only interested in formulas for the Green function that are ready for applications are referred to Sec. S8 for a summary.

S1. EMBEDDING COORDINATES

In this section, we explain how the finite graph with ℓ rings is embedded into the Poincaré disk.

We assign a coordinate $z_i \in \mathbb{D}$ to each graph site $i \in G$ such that neighboring sites are at hyperbolic distance d_0 , with d_0 to be determined. In order to label the coordinates $z_i \in \mathbb{D}$, we have in mind the topologically equivalent graph with ℓ concentric rings, See Fig. 1. We enumerate the N graph sites with an index i in a counterclockwise manner by starting on the first ring, then the second ring, and so forth. In this way, the first $i = 1, \dots, 7$ sites are on ring $\ell = 1$, sites $i = 8, \dots, 35$ are on ring $\ell = 2$, etc. The number of sites on each ring are summarized in Table II.

The construction of the tessellation starts with the central regular heptagon with $|z_1| = \dots |z_7| = r_0$. For a general hyperbolic lattice $\{p, q\}$ we have

$$r_0 = \sqrt{\frac{\cos(\frac{\pi}{q} + \frac{\pi}{p})}{\cos(\frac{\pi}{p} - \frac{\pi}{q})}} \quad (\text{S1})$$

ℓ rings	1	2	3	4	5	6	7	8
$N_{\text{ring}}(\ell)$	7	28	77	203	532	1393	3647	9548
$N(\ell)$	7	35	112	315	847	2240	5887	15435

TABLE II. Number of sites on the ℓ th ring, $N_{\text{ring}}(\ell)$, and total number of sites for a graph with ℓ rings, $N(\ell)$, for the first eight rings.

and so for our tessellation $\{7, 3\}$ we find

$$r_0 = 0.300743. \quad (\text{S2})$$

In particular, the first two coordinates are $z_1 = r_0$ and $z_2 = r_0 e^{2\pi i/7}$ so that

$$d_0 = d(z_1, z_2) = 0.283128 \quad (\text{S3})$$

with $d(z, z')$ the hyperbolic distance in the Poincaré disk. Starting from the central heptagon, the hyperbolic lattice is generated by iteratively applying the two generators of the symmetry group of the tessellation to the existing sites, which are rotations by $2\pi/7$ through the center of a heptagon and rotations by $2\pi/3$ through a vertex. Alternatively, we can create polygons by iteratively inverting existing polygons on hyperbolic circles along the edges of the polygon.

A list of coordinates $\{z_i\}$ for the sites of the first $\ell = 6$ rings is attached to this work as supplementary data in the file “coordinates.dat” [53]. The file contains 2240 lines, which correspond to the 2240 coordinates for the graph with six rings. The first (second) column of the data constitutes the real (imaginary) part of $z_i \in \mathbb{D}$. In order to extract the coordinates for a graph with $\ell = 1, 2, 3, 4, 5, 6$ rings, restrict to the first 7, 35, 112, 315, 827, 2240 lines of the data, respectively.

S2. DERIVATION OF EQ. (7) AND CORRECTIONS

In this section we present a more detailed derivation of Eq. (7) for approximating the adjacency matrix by the hyperbolic Laplacian. We further discuss the validity of this relation for boundary sites with coordination number 2 and compute the next-to-leading order correction in the expansion in powers of h .

Derivation of Eq. (7). Choose an arbitrary site z_i of the hyperbolic lattice with coordination number 3. For a test function $f : \mathbb{D} \rightarrow \mathbb{C}$ such that $f(z_i) = f_i$ we then have

$$A_{ij} f_j = f(z_{i+e_1}) + f(z_{i+e_2}) + f(z_{i+e_3}), \quad (\text{S4})$$

where z_{i+e_a} with $a = 1, 2, 3$ stands for the sites adjacent to z_i . The heptagonal lattice is such that all adjacent lattice sites have the same distance with respect to the hyperbolic metric. In particular, this property remains

invariant under automorphisms of the Poincaré disk. We apply the transformation $\mathbb{D} \rightarrow \mathbb{D}$,

$$z \mapsto w(z) = \frac{z_i - z}{1 - z\bar{z}_i}, \quad (\text{S5})$$

$$w \mapsto z(w) = \frac{z_i - w}{1 - w\bar{z}_i}, \quad (\text{S6})$$

which exchanges z_i and the origin. We write $f(z) = \tilde{f}(w(z))$ and have

$$A_{ij}f_j = \tilde{f}(w(z_{i+e_1})) + \tilde{f}(w(z_{i+e_2})) + \tilde{f}(w(z_{i+e_3})). \quad (\text{S7})$$

The adjacent sites in the rotated frame, however, have very simple coordinates: Modulo rotation, they correspond to three sites at hyperbolic distance d_0 from the origin, with mutual relative angle $2\pi/3$. The corresponding Euclidean distance h in the disk is such that

$$d(h, 0) \stackrel{!}{=} d_0, \quad (\text{S8})$$

and so

$$h = \tanh(d_0) = 0.275798. \quad (\text{S9})$$

We write

$$w_1 = w(z_{i+e_1}) = he^{i\chi_i}, \quad (\text{S10})$$

$$w_2 = w(z_{i+e_2}) = he^{i2\pi/3}e^{i\chi_i}, \quad (\text{S11})$$

$$w_3 = w(z_{i+e_3}) = he^{i4\pi/3}e^{i\chi_i}, \quad (\text{S12})$$

where the angle χ_i is determined by the coordinate z_i , see below. We have

$$w_1 + w_2 + w_3 = w_1^2 + w_2^2 + w_3^2 = 0. \quad (\text{S13})$$

Applying the inverse automorphism we can parametrize the sites adjacent to z_i as

$$z_{i+e_1} = z(w_1) = \frac{z_i - w_1}{1 - w_1\bar{z}_i}, \quad (\text{S14})$$

$$z_{i+e_2} = z(w_2) = \frac{z_i - w_2}{1 - w_2\bar{z}_i}, \quad (\text{S15})$$

$$z_{i+e_3} = z(w_3) = \frac{z_i - w_3}{1 - w_3\bar{z}_i} \quad (\text{S16})$$

and so

$$A_{ij}f_j = f\left(\frac{z_i - w_1}{1 - w_1\bar{z}_i}\right) + f\left(\frac{z_i - w_2}{1 - w_2\bar{z}_i}\right) + f\left(\frac{z_i - w_3}{1 - w_3\bar{z}_i}\right). \quad (\text{S17})$$

The right-hand side is a complex number that depends on the parameter h and can be approximated through Taylor's formulas by a polynomial in h . We write

$$A_{ij}f_j = 3f(z_i) + Q_1h + Q_2h^2 + \mathcal{O}(h^3) \quad (\text{S18})$$

with

$$Q_1 = \frac{d}{dh} \left[f\left(\frac{z_i - w_1}{1 - w_1\bar{z}_i}\right) + f\left(\frac{z_i - w_2}{1 - w_2\bar{z}_i}\right) + f\left(\frac{z_i - w_3}{1 - w_3\bar{z}_i}\right) \right]_{h=0}, \quad (\text{S19})$$

$$Q_2 = \frac{1}{2} \frac{d^2}{dh^2} \left[f\left(\frac{z_i - w_1}{1 - w_1\bar{z}_i}\right) + f\left(\frac{z_i - w_2}{1 - w_2\bar{z}_i}\right) + f\left(\frac{z_i - w_3}{1 - w_3\bar{z}_i}\right) \right]_{h=0}. \quad (\text{S20})$$

We use a complex notation where we identify $f(z) \equiv f(z, \bar{z})$ and

$$\partial_z = \frac{\partial}{\partial z} = \frac{1}{2}(\partial_x - i\partial_y), \quad (\text{S21})$$

$$\bar{\partial}_z = \frac{\partial}{\partial \bar{z}} = \frac{1}{2}(\partial_x + i\partial_y). \quad (\text{S22})$$

For $a = 1, 2, 3$ (with $w_{a,h} := dw_a/dh = w_a/h$) we arrive at

$$\begin{aligned} & \frac{d}{dh} f\left(\frac{z_i - w_a}{1 - w_a\bar{z}_i}\right)_{h=0} \\ &= -(1 - |z_i|^2) \left(w_{1,h} \partial_z + \bar{w}_{1,h} \bar{\partial}_z \right) f(z_i), \end{aligned} \quad (\text{S23})$$

$$\begin{aligned} & \frac{d^2}{dh^2} f\left(\frac{z_i - w_a}{1 - w_a\bar{z}_i}\right)_{h=0} \\ &= (1 - |z_i|^2)^2 \left(\partial_z^2 f(z_i) w_{1,h}^2 + \bar{\partial}_z^2 f(z_i) \bar{w}_{1,h}^2 \right) \\ & \quad - 2\bar{z}_i(1 - |z_i|^2) w_{1,h}^2 \partial_z f(z_i) - 2z_i(1 - |z_i|^2) \bar{w}_{1,h}^2 \bar{\partial}_z f(z_i) \\ & \quad + 2(1 - |z_i|^2)^2 |w_{1,h}|^2 \partial_z \bar{\partial}_z f(z_i). \end{aligned} \quad (\text{S24})$$

Summing over the index a and using $\sum_{a=1}^3 w_a = \sum_{a=1}^2 w_a^2 = 0$ and $|w_{a,h}| = 1$ this implies

$$Q_1 = 0 \quad (\text{S25})$$

and

$$Q_2 = 3(1 - |z_i|^2)^2 \partial_z \bar{\partial}_z f(z_i). \quad (\text{S26})$$

Note that $\Delta = 4\partial_z \bar{\partial}_z$. Thus we have shown that

$$A_{ij}f_j = 3f(z_i) + \frac{3}{4}h^2 \Delta_g f(z_i) + \mathcal{O}(h^3) \quad (\text{S27})$$

for a site with coordination number 3.

Coordination number 2. Any site z_i with coordination number 2 necessarily lies on the boundary of the graph, which we assume to be built from ℓ rings. Denote the two sites adjacent to z_i in G by z_{i+e_1} and z_{i+e_2} . The coordinate of the third neighboring site z_{i+e_3} lies on the $(\ell+1)$ th ring outside G , but is otherwise uniquely specified by the heptagonal tessellation of the hyperbolic plane. We then

have

$$\begin{aligned}
A_{ij}f(z_i) &= f(z_{i+e_1}) + f(z_{i+e_2}) \\
&= \underbrace{[-f(z_{i+e_3}) + f(z_{i+e_3})]}_0 + f(z_{i+e_1}) + f(z_{i+e_2}) \\
&= -f(z_{i+e_3}) + 3f(z_i) + \frac{3}{4}h^2\Delta_g f(z_i) + \mathcal{O}(h^3).
\end{aligned} \tag{S28}$$

We could now expand the first term to linear order in h , giving $f(z_{i+e_3}) = f(z_i) + h \cdot \delta_n f(z_i)$, with $\delta_n f(z_i)$ a directional derivative along the line from z_i to z_{i+e_3} . On the other hand, for our purposes we need Eq. (S27) only for the case that $f_i = \hat{a}_i = \hat{\alpha}(z_i)$ is an annihilation operator. For any many-body state $|\Psi\rangle$ describing the system on graph G we have $\hat{\alpha}_{i+e_3}|\Psi\rangle = 0$, since $z_{i+e_3} \notin G$. Consequently

$$A_{ij}\hat{a}_j|\Psi\rangle = \left(3\hat{\alpha}(z_i) + \frac{3}{4}h^2\Delta_g\hat{\alpha}(z_i)\right)|\Psi\rangle + \mathcal{O}(h^3), \tag{S29}$$

and so the linear term should not affect observables. We leave the detailed analysis of these boundary effects to future work, since obviously they do not significantly affect the accuracy of the observables computed in this work.

Third order in h . It is further possible to determine the coefficient Q_3 in the expansion

$$A_{ij}f_j = 3f(z_i) + \frac{3}{4}h^2\Delta_g f(z_i) + Q_3h^3 + \mathcal{O}(h^4) \tag{S30}$$

along the same lines. We have

$$Q_3 = \frac{1}{2} \left[e^{3i\chi_i} \mathcal{D}f(z_i) + e^{-3i\chi_i} \bar{\mathcal{D}}f(z_i) \right] \tag{S31}$$

with differential operator

$$\mathcal{D} = \partial_z^2 (1 - |z|^2)^3 \partial_{\bar{z}}. \tag{S32}$$

To understand the role of α_i in this formula, it is instructive to express ∂_z in radial coordinates according to

$$\partial_z = \frac{e^{-i\phi}}{2} \left(\partial_r - \frac{i}{r} \partial_\phi \right). \tag{S33}$$

Consequently only the combination

$$\delta_i = \chi_i - \phi_i \tag{S34}$$

is relevant when applying \mathcal{D} in Eq. (S24). We find that δ_i in most cases (not all) only depends on the radius r_i , and is wildly fluctuating as we go from one lattice site to the other, see Fig. 4. This may explain why the contributions of the operator \mathcal{D} , although only suppressed by a power of h , seem to be unimportant for computing the observables we consider in this work.

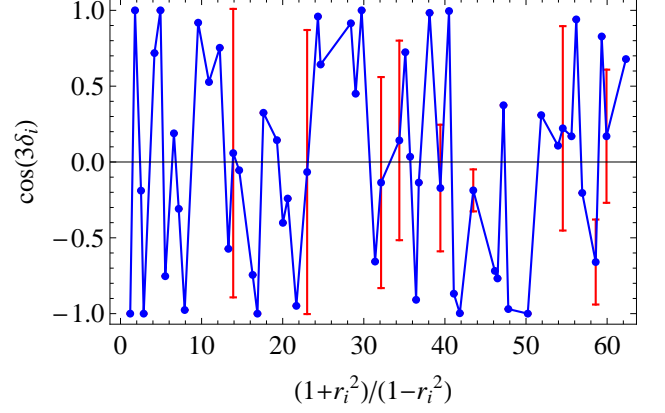


FIG. 4. The angle $\delta_i = \chi_i - \phi_i$ is heavily oscillating between sites with nearby radius. In most cases, δ_i only depends on the value of the radius $|z_i| = r_i$. Here we plot the averaged angle δ_i vs. site radius r_i for the first 5 rings (comprising 847 sites). The red “error bars” indicate those cases where the mapping $\delta_i \rightarrow r_i$ is not unique. Still, for any given site i we can unambiguously assign the value of δ_i through Eqs. (S10)-(S12).

S3. DERIVATION OF EQS. (8) AND (9)

In this section we show how sums of the type

$$\sum_{i \in G} f(z_i) \tag{S35}$$

with a suitable function $f(z)$ can be approximated by integrals over the Poincaré disk with a finite radius $L < 1$. We assume the graph G to consist of ℓ rings.

To simplify the matter let us first assume that $f(z)$ only depends on $r = |z|$. Define the counting function

$$\mathcal{N}(r) = \sum_{i \in G} \Theta(r - r_i). \tag{S36}$$

Further introduce the hyperbolic invariant ρ via

$$\rho = \frac{1 + r^2}{1 - r^2}, \quad d\rho = 4 \frac{dr}{(1 - r^2)^2}. \tag{S37}$$

We find that $\mathcal{N}(r)$ is approximately linear in ρ and given by

$$\mathcal{N}(r) \approx 14\rho + b, \tag{S38}$$

with b a constant, see Fig. 5. Hence $d\mathcal{N}(r) = 14d\rho$. In order to approximate the finite sum by a compactly supported integral, we restrict the integration to a disk

of radius $L < 1$, with L to be determined. We have

$$\begin{aligned} \sum_{i \in G} f(r_i) &\approx \int dN(r) f(r) = 14 \int d\rho f(r) \\ &= 14 \cdot 4 \int_0^L \frac{dr r}{(1-r^2)^2} f(r) \\ &= \frac{14 \cdot 4}{2\pi} \int_{|z| \leq L} \frac{d^2 z}{(1-|z|^2)^2} f(|z|). \end{aligned} \quad (\text{S39})$$

We fix the effective radius L by matching the total number of sites N to the right-hand side $\frac{14 \cdot 4}{2\pi} \frac{\pi L^2}{1-L^2}$ for $f(r) = 1$. This yields

$$L = \sqrt{\frac{N}{N+28}}. \quad (\text{S40})$$

In order to approximate the angular dependence for a more general function $f(z) = f(re^{i\phi})$ we can employ standard arguments from Riemann integration. Due to the sevenfold rotation invariance of the lattice we can divide the N lattice sites $\{i \in G\}$ into $N/7$ “shells”, labelled $[i]$, where each shell contains seven sites with equal radius r_i and angle $\phi_i + 2\pi j/7$ with $j = 0, \dots, 6$. Summing over these seven sites for fixed r_i we have

$$\sum_{j=0}^6 f(r_i e^{i\phi_i + 2\pi i j/7}) \approx 7 \int_0^{2\pi} \frac{d\phi}{2\pi} f(r_i e^{i\phi}), \quad (\text{S41})$$

where we approximated the sum by a Riemann integral. For the total sum over lattice sites we then have

$$\begin{aligned} \sum_{i \in G} f(r_i e^{i\phi_i}) &= \sum_{[i]} \sum_{j=0}^6 f(r_i e^{i\phi_i + 2\pi i j/7}) \\ &\approx \int_0^{2\pi} \frac{d\phi}{2\pi} \left(\sum_{[i]} 7 f(r_i e^{i\phi}) \right) \\ &= \int_0^{2\pi} \frac{d\phi}{2\pi} \sum_{i \in G} f(r_i e^{i\phi}) \\ &\approx \int_0^{2\pi} \frac{d\phi}{2\pi} \cdot 14 \cdot 4 \int_0^L \frac{dr r}{(1-r^2)^2} f(re^{i\phi}) \\ &= \frac{14 \cdot 4}{2\pi} \int_{|z| \leq L} \frac{d^2 z}{(1-|z|^2)^2} f(z). \end{aligned} \quad (\text{S42})$$

This shows that Eq. (S39) generalizes to functions with nontrivial angular dependence.

S5. EIGENFUNCTIONS OF HYPERBOLIC LAPLACIAN

In this section we summarize the spectral properties of the hyperbolic Laplacian, i.e. the eigenvalues and eigenfunctions in different representations.

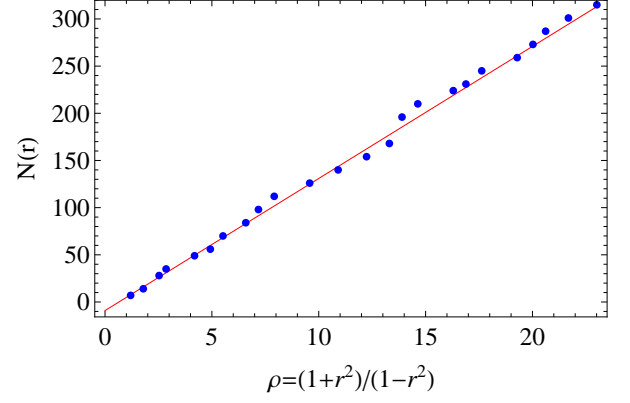


FIG. 5. Counting function $\mathcal{N}(r)$ for radii within the first $\ell = 4$ rings versus the linear curve $14\rho + b$, with $b = -9.096$.

We label the eigenfunctions of Δ_g on the Poincaré disk by a momentum parameter

$$K = k e^{i\beta} \quad (\text{S43})$$

with $k \geq 0$ the amplitude and $\beta \in [0, 2\pi)$ a phase. The corresponding eigenfunction is

$$\psi_K(z) = \left(\frac{1-|z|^2}{|1-ze^{-i\beta}|^2} \right)^{\frac{1}{2}(1+ik)}, \quad (\text{S44})$$

and applying $\Delta_g = 4(1-|z|^2)^2 \partial_z \bar{\partial}_z$ it is easy to see that the corresponding eigenvalue is

$$\varepsilon_K = -(k^2 + 1). \quad (\text{S45})$$

The norm of ψ_K for a disk of radius $L < 1$ is

$$\|\psi_K\|^2 = \int_{|z| \leq L} \frac{d^2 z}{(1-|z|^2)^2} |\psi_K(z)|^2 = \frac{\pi L^2}{1-L^2}, \quad (\text{S46})$$

which is the hyperbolic volume of the disk. Note how this is analogous to the Euclidean case. Indeed, the Euclidean plane wave solutions

$$\psi_K(z) \simeq e^{i\mathbf{k} \cdot \mathbf{x}} = \exp \left[\frac{i}{2} (K\bar{z} + \bar{K}z) \right] \quad (\text{S47})$$

are recovered for $z \ll 1$ and $k \gg 1$, which corresponds to the radius of the Poincaré disk approaching infinity and hence vanishing curvature.

Often it is advantageous to express the eigenfunction in radial coordinates $z = re^{i\phi}$. For $k \geq 0$ and $m \in \mathbb{Z}$ we define the radial eigenfunctions $g_{km}(r)$ corresponding to the eigenvalue $-(k^2 + 1)$ such that

$$\psi_K(z) = \sum_{m=-\infty}^{\infty} i^m g_{km}(r) e^{im(\phi-\beta)}. \quad (\text{S48})$$

The ansatz is motivated by the Euclidean formula

$$e^{i\mathbf{k} \cdot \mathbf{x}} = \sum_{m=-\infty}^{\infty} i^m J_m(kr) e^{im(\phi-\beta)} \quad (\text{S49})$$

with Bessel functions J_m . We have

$$g_{km}(r) = i^{-m} \int_0^{2\pi} \frac{d\phi}{2\pi} e^{-im\phi} \left(\frac{1-r^2}{|1-re^{i\phi}|^2} \right)^{\frac{1}{2}(1+ik)}, \quad (\text{S50})$$

which can be solved numerically. However, the functions $g_{km}(r)$ can be determined in closed form by making the ansatz $g_{km}(r) = \hat{g}(\frac{1+r^2}{1-r^2})$, which leads to Legendre's differential equation (S90) for \hat{g} . This yields

$$g_{km}(r) \propto P_\nu^m \left(\frac{1+r^2}{1-r^2} \right) \quad (\text{S51})$$

with $\nu = \frac{1}{2}(-1+ik)$ and P_ν^m the Legendre function of the first kind. The correct prefactor ensuring Eq. (S48) is found to be

$$\begin{aligned} g_{k,m=0}(r) &= P_\nu \left(\frac{1+r^2}{1-r^2} \right), \\ g_{k,m>0}(r) &= \frac{1}{\prod_{n=0}^{m-1} (\nu-n)} P_\nu^m \left(\frac{1+r^2}{1-r^2} \right), \\ g_{k,m<0}(r) &= (-1)^m g_{k,m>0}(r). \end{aligned} \quad (\text{S52})$$

In the Euclidean limit $r \ll 1$ and $k \gg 1$ we recover $\bar{g}_{km}(r) \simeq J_m(kr)$.

S6. COMPUTATION OF LOWEST EIGENVALUES AND DERIVATION OF EQ. (14)

In this section we give details for the determination of the ground state energy and spectral gap of (1) the Hamiltonian $H = -A$ on a graph with ℓ rings and (2) its continuum approximation $H^{(\text{cont})} = -3 - \frac{3}{4}h^3\Delta_g$ on a disk of radius $L = \sqrt{N/(N+24)}$.

Graph Hamiltonian. Denote the lowest two eigenvalues of H by E_0 and $E_1 > E_0$. For moderately sized $\ell \lesssim 7$ we easily find the spectrum of A using matrix diagonalization. For larger $\ell \geq 8$, due to the exponential increase in the size of the matrix, we use sparse matrix techniques to determine the lowest two eigenvalues. Specifically, we employ the numerical Lanczos algorithm to estimate E_0 and E_1 , and estimate the results to be reliable to about three significant digits. Note that the accuracy of the algorithm becomes worse as the spacing between E_0 and E_1 becomes smaller. Since a more precise determination of the values of E_0 and E_1 is not among the goals of the present work, we are not able to test whether the relative error between $E_{0,1}$ and $E_{0,1}^{(\text{cont})}$ decreases as $\ell \rightarrow \infty$. The results are summarized in Table III.

Continuous Hamiltonian. The eigenvalues of $H^{(\text{cont})}$ read

$$E_{nm} = -3 + \frac{3}{4}h^2(k_{nm}^2 + 1), \quad (\text{S53})$$

where k_{nm} satisfies the Dirichlet boundary condition

$$P_{\nu_{nm}}^m \left(\frac{1+L^2}{1-L^2} \right) = 0 \quad (\text{S54})$$

with Legendre function of the first kind P_ν^m and $\nu_{nm} = \frac{1}{2}(-1+ik_{nm})$. We label the eigenenergies by $n = 1, 2, 3, \dots$ and $m \in \mathbb{Z}$. The ground and first excited state have azimuthal quantum numbers $m = 0$ and $m = 1$, respectively. In order to declutter notation in the following we define

$$k_0 = k_{1,0}, \quad E_0^{(\text{cont})} = -3 + \frac{3}{4}h^2(k_0^2 + 1), \quad (\text{S55})$$

$$k_1 = k_{1,1}, \quad E_1^{(\text{cont})} = -3 + \frac{3}{4}h^2(k_1^2 + 1). \quad (\text{S56})$$

Equation (S54) is readily solved numerically and we present the lowest two eigenvalues $E_0^{(\text{cont})}$ and $E_1^{(\text{cont})}$ in Table III.

We can employ Eq. (S54) to compute the asymptotic behavior of k_0 as $L \rightarrow 1$ (or equivalently $\ell \rightarrow \infty$). For large $x \rightarrow \infty$ we have

$$\begin{aligned} P_\nu(x \rightarrow \infty) &\sim \left(\frac{2}{x} \right)^{\frac{1}{2}(1+ik)} \frac{\Gamma(-ik)}{\Gamma(\frac{1}{2}(1-ik))^2} \\ &\quad + \left(\frac{2}{x} \right)^{\frac{1}{2}(1-ik)} \frac{\Gamma(ik)}{\Gamma(\frac{1}{2}(1+ik))^2} \end{aligned} \quad (\text{S57})$$

with Euler's Γ -function. In order to find the zeros we consider the amplitude

$$\begin{aligned} |P_\nu(x \rightarrow \infty)|^2 &\sim \frac{2}{x} \left| \frac{\Gamma(-ik)}{\Gamma(\frac{1}{2}(1-ik))^2} \right|^2 \\ &\quad \times \left| 1 + \left(\frac{2}{x} \right)^{-ik} \frac{\Gamma(ik)\Gamma(\frac{1}{2}(1-ik))^2}{\Gamma(-ik)\Gamma(\frac{1}{2}(1+ik))^2} \right|^2 \\ &= \frac{2 \cosh^2(\pi k/2)}{x \pi k \sinh(\pi k)} \times \left| 1 + \left(\frac{2}{x} \right)^{-ik} e^{i\Phi(k)} \right|^2 \end{aligned} \quad (\text{S58})$$

with

$$i\Phi(k) = \ln \left(\frac{\Gamma(ik)\Gamma(\frac{1}{2}(1-ik))^2}{\Gamma(-ik)\Gamma(\frac{1}{2}(1+ik))^2} \right). \quad (\text{S59})$$

The first term in Eq. (S58) is positive. Thus the lowest zero k_0 for $L \rightarrow 1$ follows from

$$\begin{aligned} \pi &\stackrel{!}{=} -k_0 \ln \left(\frac{2}{x} \right) + \Phi(k_0) \\ &= -k_0 \ln \left(\frac{2}{x} \right) - \pi + 4k_0 \ln 2 + \mathcal{O}(k^3) \\ &= -\pi + k_0 \ln(8x) + \mathcal{O}(k^3) \end{aligned} \quad (\text{S60})$$

for $x = \frac{1+L^2}{1-L^2} \rightarrow \infty$. Consequently,

$$k_0 \sim \frac{2\pi}{\ln(8\frac{1+L^2}{1-L^2})} \simeq \frac{\pi}{\ln(2\varphi^\ell)}. \quad (\text{S61})$$

We inserted $N \sim 7\varphi^{2\ell}$ with golden ratio $\varphi = (1+\sqrt{5})/2$ such that $\frac{1+L^2}{1-L^2} \sim \frac{1}{2}\varphi^{2\ell}$. The ground state energy for large ℓ follows as

$$E_0^{(\text{cont})} \sim -3 + \frac{3}{4}h^2 + \frac{3\pi^2 h^2}{4} \frac{1}{[\ln \varphi \cdot \ell + \ln 2]^2} \quad (\text{S62})$$

ℓ	1	2	3	4	5	6	7	8	9	10
E_0	-2	-2.636	-2.787	-2.847	-2.877	-2.894	-2.905	-2.91	-2.92	-2.92
exact $E_0^{(\text{cont})}$	-1.500	-2.570	-2.770	-2.842	-2.876	-2.895	-2.906	-2.914	-2.920	-2.924
asymptotic $E_0^{(\text{cont})}$	-2.535	-2.738	-2.820	-2.861	-2.884	-2.899	-2.909	-2.916	-2.921	-2.924
E_1	-1.274	-2.283	-2.627	-2.762	-2.827	-2.863	-2.884	-2.90	-2.91	-2.91
exact $E_1^{(\text{cont})}$	0.620	-2.085	-2.578	-2.746	-2.821	-2.861	-2.884	-2.899	-2.908	-2.915
asymptotic $E_1^{(\text{cont})}$	15.58	-1.633	-2.507	-2.728	-2.815	-2.858	-2.883	-2.898	-2.908	-2.915

TABLE III. We compare the ground and first excited state energies for the graph and conitnuum for $\ell = 1, \dots, 10$. The “asymptotic” continuum formulas for $E_0^{(\text{cont})}$ and $E_1^{(\text{cont})}$ correspond to Eqs. (S62) and (S68), respectively. For $\ell \geq 8$ we give an estimate of E_0 and E_1 from sparse matrix methods.

The first excited state energy of $H^{(\text{cont})}$ can be determined in a fully analogous way from

$$P_{\nu_1}^1 \left(\frac{1+L^2}{1-L^2} \right), \quad \nu_1 = \frac{1}{2}(-1 + ik_1). \quad (\text{S63})$$

We have

$$|P_{\nu}^1(x \rightarrow \infty)|^2 \propto \left| 1 + \left(\frac{2}{x} \right)^{-ik} e^{i\Phi_1(k)} \right|^2 \quad (\text{S64})$$

with

$$i\Phi_1(k) = \ln \left(\frac{\Gamma(ik)\Gamma(\frac{1}{2}(1-ik))\Gamma(\frac{1}{2}(-1-ik))}{\Gamma(-ik)\Gamma(\frac{1}{2}(1+ik))\Gamma(\frac{1}{2}(-1+ik))} \right). \quad (\text{S65})$$

Hence k_1 for $x = \frac{1+L^2}{1-L^2} \rightarrow \infty$ is found from

$$\begin{aligned} \pi &\stackrel{!}{=} -k_1 \ln \left(\frac{2}{x} \right) + \Phi_1(k_1) \\ &= -k_1 \ln \left(\frac{2}{x} \right) - \pi + 2[2 \ln 2 - 1]k_1 + \mathcal{O}(k_1^3) \\ &= -\pi - k_1 \ln \left(\frac{8x}{e^2} \right) + \mathcal{O}(k_1^3). \end{aligned} \quad (\text{S66})$$

This implies

$$k_1 \sim \frac{2\pi}{\ln \left(\frac{8}{e^2} \frac{1+L^2}{1-L^2} \right)} \simeq \frac{\pi}{\ln \left(\frac{2}{e} \varphi^\ell \right)} \quad (\text{S67})$$

and

$$E_1^{(\text{cont})} \sim -3 + \frac{3}{4}h^2 + \frac{3\pi^2 h^2}{4} \frac{1}{[\ln \varphi \cdot + \ln 2 - 1]^2}. \quad (\text{S68})$$

S4. DERIVATION OF EQ. (16)

In this section we derive the relation between the graph green function $G_{ij}(\omega)$ and the continuum Green function $G(z, z', \lambda, L)$ using an auxiliary field path integral representation.

We first recall some path integral identities [62]. If θ_i is a discrete real variable and M_{ij} a real and symmetric matrix then

$$\langle \theta_i \theta_j \rangle := \frac{\int \mathcal{D}\theta \theta_i \theta_j e^{-\frac{1}{2} \theta_k M_{kl} \theta_l}}{\int \mathcal{D}\theta e^{-\frac{1}{2} \theta_k M_{kl} \theta_l}} = (M^{-1})_{ij} \quad (\text{S69})$$

with $\mathcal{D}\theta = \prod_i d\theta_i$. Furthermore, if $\theta(x)$ is a real field and \hat{D} a differential operator, then $\mathcal{D}\theta = \prod_x d\theta(x)$ and

$$\langle \theta(x) \theta(y) \rangle := \frac{\int \mathcal{D}\theta \theta(x) \theta(y) e^{-\frac{1}{2} \int d^d r \theta \hat{D} \theta}}{\int \mathcal{D}\theta e^{-\frac{1}{2} \int d^d r \theta \hat{D} \theta}} = -G(x, y), \quad (\text{S70})$$

where $G(x, y)$ is the Green function of \hat{D} according to

$$\hat{D}G(x, y) = -\delta^{(d)}(x - y). \quad (\text{S71})$$

This can be applied to match the Green function on the graph G_{ij} to the continuum Green function $G(z, z')$ evaluated on the graph sites. The graph Green function is given by

$$G_{ij}(\omega, \ell) = \left(\frac{1}{H - \omega \mathbb{1}} \right)_{ij} = \sum_{n=1}^N \frac{\psi_n(z_i) \psi_n^*(z_j)}{\varepsilon_n - \omega} \quad (\text{S72})$$

with $H = -A$ and $H\psi_n = \varepsilon_n \psi_n$. Introduce the auxiliary real field $\theta_i \rightarrow \theta(z_i)$ and approximate $H \approx -3 - \frac{3}{4}h^2 \Delta_g$ and $\sum_i \approx \frac{28}{\pi} \int_{|z| \leq L} \frac{d^2 z}{(1-|z|^2)^2}$ to find

$$\begin{aligned}
G_{ij}(\omega, \ell) &= \frac{\int D\theta \theta_i \theta_j \exp\left[-\frac{1}{2} \sum_{i,j} \theta_i (H - \omega \mathbb{1})_{ij} \theta_j\right]}{\int D\theta \exp\left[-\frac{1}{2} \sum_{i,j} \theta_i (H - \omega \mathbb{1})_{ij} \theta_j\right]} \\
&= \frac{\int D\theta \theta_i \theta_j \exp\left[-\frac{1}{2} \sum_{i,j} \theta_i [(3\mathbb{1} - A) - (\omega + 3)\mathbb{1}]_{ij} \theta_j\right]}{\int D\theta \exp\left[-\frac{1}{2} \sum_{i,j} \theta_i [(3\mathbb{1} - A) - (\omega + 3)\mathbb{1}]_{ij} \theta_j\right]} \\
&\approx \frac{\int D\theta \theta(z_i) \theta(z_j) \exp\left[-\frac{1}{2} \frac{28}{\pi} \int_{|z| \leq L} \frac{d^2 z}{(1-|z|^2)^2} \theta(z) \left[-\frac{3h^2}{4} \Delta_g - (\omega + 3)\right] \theta(z)\right]}{\int D\theta \exp\left[-\frac{1}{2} \frac{28}{\pi} \int_{|z| \leq L} \frac{d^2 z}{(1-|z|^2)^2} \theta(z) \left[-\frac{3h^2}{4} \Delta_g - (\omega + 3)\right] \theta(z)\right]} \\
&= \frac{\int D\theta \theta(z_i) \theta(z_j) \exp\left[-\frac{1}{2} C' \int_{|z| \leq L} \frac{d^2 z}{(1-|z|^2)^2} \theta(z) [-\Delta_g - \lambda] \theta(z)\right]}{\int D\theta \exp\left[-\frac{1}{2} C' \int_{|z| \leq L} \frac{d^2 z}{(1-|z|^2)^2} \theta(z) [-\Delta_g - \lambda] \theta(z)\right]} \\
&= \frac{1}{C'} G(z_i, z_j, \lambda, L)
\end{aligned} \tag{S73}$$

with

$$C' = \frac{3h^2}{4} \frac{28}{\pi} = \frac{21h^2}{\pi} = 0.508, \quad \lambda = \frac{4(\omega + 3)}{3h^2}. \tag{S74}$$

Here $G(z, z', \lambda, L)$ is the hyperbolic Green function of $(\Delta_g + \lambda)$ on a disk of radius L , i.e.

$$\frac{1}{(1-|z|^2)^2} (\Delta_g + \lambda) G(z, z', \lambda, L) = -\delta^{(2)}(z - z'). \tag{S75}$$

We conclude

$$G_{ij}(\omega, \ell) = \frac{\pi}{21h^2} G\left(z_i, z_j, \lambda = \frac{4(\omega + 3)}{3h^2}, L\right). \tag{S76}$$

S7. CONTINUUM GREEN FUNCTION (COMPUTATION)

In this section, we compute Green's functions for the hyperbolic Laplacian Δ_g and hyperbolic Helmholtz operator $\lambda + \Delta_g$ (with $\lambda \in \mathbb{C}$) on the disk of radius $L \leq 1$ with Dirichlet boundary conditions. A self-contained summary of the relevant formulas is given in the next section.

Definition. The Green function is defined by

$$(\lambda + \Delta_g) G(z, z', \lambda, L) = -(1 - |z|^2)^2 \delta^{(2)}(z - z') \tag{S77}$$

with $\Delta_g = (1 - |z|^2)^2 4\partial_z \bar{\partial}_z$ acting on z and Dirichlet boundary conditions such that $G(z, z', \lambda, L) = 0$ for $|z| = L$ or $|z'| = L$. Here $(1 - |z|^2)^2 \delta^{(2)}(z - z')$ is the δ -function with respect to the hyperbolic volume measure. For an arbitrary continuous function $f : \mathbb{D} \rightarrow \mathbb{C}$ it is defined by

$$\int_{\mathbb{D}} \frac{d^2 z}{(1 - |z|^2)^2} (1 - |z|^2)^2 \delta^{(2)}(z - z') f(z) = f(z'). \tag{S78}$$

In Cartesian coordinates such that $z = x + iy$ we have $d^2 z = dx dy$ and $\delta^{(2)}(z - z') = \delta(x - x') \delta(y - y')$.

Spectral representation. It is always possible to give a closed expression for the Green function in terms of the spectral decomposition of the operator. For this write the eigenfunctions of the hyperbolic Laplacian in radial coordinates by $g_{km}(r) e^{im\phi}$ with g_{km} from Eq. (S52). The normalized eigenfunctions of Δ_g on the disk of radius $L < 1$ are given

$$\psi_{nm}(z) = \frac{g_{k_{nm}m}(r) e^{im\phi}}{\|g_{k_{nm}m}\|}, \tag{S79}$$

where k_{nm} solves $g_{k_{nm}m}(L) = 0$ and the norm is

$$\|g_{km}\|^2 = 2\pi \int_0^L \frac{dr r}{(1 - r^2)^2} |g_{km}(r)|^2. \tag{S80}$$

The Green function can then be written in spectral representation as

$$G(z, z', \lambda, L) = \sum_{m=-\infty}^{\infty} \sum_n \frac{\psi_{nm}(z) \psi_{nm}^*(z')}{-\lambda + k_{nm}^2 + 1}. \tag{S81}$$

Equation (S77) follows from the completeness of the eigenfunctions and the Dirichlet boundary condition is satisfied due to $\psi_{nm}(z) = 0$ for $|z| = L$. However, the spectral representation is not the most useful form of the Green function since it requires to determine the discrete momenta k_{nm} and subsequently to perform the double-sum numerically. Thus we derive a few complementary expressions in the following.

Hyperbolic Laplacian. First consider the case $\lambda = 0$, where Eq. (S77) reduces to

$$\Delta_g G(z, z', 0, L) = -(1 - |z|^2)^2 \delta^{(2)}(z - z'). \tag{S82}$$

We divide by $(1 - |z|^2)^2$ and observe that $G(z, z', 0, L)$ coincides with the Green function of the ordinary Laplacian Δ on a disk of radius $L < 1$. The latter is given by

$$G(z, z', 0, L) = -\frac{1}{4\pi} \ln |z - z'|^2 + \delta G(z, z', 0, L), \quad (\text{S83})$$

where the first term is the fundamental solution, while the second term is a harmonic function ensuring Dirichlet boundary conditions. We construct δG from a mirror charge outside the disk, whose location is obtained from inversion on the circle, $z' \rightarrow L^2/\bar{z}'$. Hence

$$\delta G(z, z', 0, L) = \frac{1}{4\pi} \ln \left| z - \frac{L^2}{\bar{z}'} \right|^2 + \text{const} \quad (\text{S84})$$

with a suitably chosen constant. We arrive at

$$G(z, z', 0, L) = -\frac{1}{4\pi} \ln \left| \frac{L(z - z')}{L^2 - z\bar{z}'} \right|^2. \quad (\text{S85})$$

For $z' = 0$ we have

$$G(r, 0, 0, L) = -\frac{1}{2\pi} \ln \left(\frac{r}{L} \right) = -\frac{1}{2\pi} \ln \left(\frac{\tanh d(r, 0)}{L} \right) \quad (\text{S86})$$

with $d(r, 0)$ the distance from the origin.

Hyperbolic Helmholtz operator. Now consider the case of arbitrary $\lambda \in \mathbb{C}$. We construct the Green function by reducing the problem to a one-dimension Sturm–Liouville problem. We refer to Appendix C of Ref. [63] for a detailed discussion of the procedure. Write

$$G(z, z', \lambda, L) = \mathcal{G}_0(z, z', \lambda) - \delta \mathcal{G}(z, z', \lambda, L), \quad (\text{S87})$$

where \mathcal{G}_0 is the fundamental solution and $\delta \mathcal{G}$ is a harmonic function to ensure Dirichlet boundary conditions. To construct these functions, we first solve, for $z \neq 0$, the equation

$$(\lambda + \Delta_g)f(z) = 0 \quad (\text{S88})$$

through an ansatz

$$f(z) = \sum_{m=-\infty}^{\infty} f_{\lambda m}(\rho) e^{im\phi} \quad (\text{S89})$$

with $\rho = \frac{1+r^2}{1-r^2}$. Then $f_{\lambda m}$ satisfies Legendre's differential equation

$$(1 - \rho^2)f''_{\lambda m} - 2\rho f'_{\lambda m} + \left(\nu(\nu + 1) - \frac{m^2}{1 - \rho^2} \right) f_{\lambda m} = 0 \quad (\text{S90})$$

with $\nu = \frac{1}{2}(-1 + i\sqrt{\lambda - 1})$ or $\frac{\lambda}{4} = -\nu(\nu + 1)$. The two linearly independent solutions are

$$u_m(\rho) = Q_{\nu}^{(m)}(\rho), \quad (\text{S91})$$

$$v_m(\rho) = P_{\nu}^{(m)}(\rho), \quad (\text{S92})$$

which are the Legendre functions of the second/first kind, being singular/regular at $\rho = 1$. Without loss of generality we assume $m \geq 0$ in the following, otherwise replace $m \rightarrow |m|$.

Introduce the Sturm–Liouville operator

$$L_m = -4 \left(\frac{d}{d\rho} \left[p(\rho) \frac{d}{d\rho} \right] + q_m(\rho) \right) \quad (\text{S93})$$

with

$$p(\rho) = (1 - \rho^2), \quad q_m(\rho) = \nu(\nu + 1) - \frac{m^2}{1 - \rho^2}. \quad (\text{S94})$$

We have

$$(\lambda + \Delta_g)f(z) = \sum_{m=-\infty}^{\infty} e^{im\phi} L_m f_{\lambda m}(\rho). \quad (\text{S95})$$

The fundamental solution of L_m is defined through

$$L_m G_m(\rho, \rho') = -4\delta(\rho - \rho'), \quad (\text{S96})$$

with the factor of 4 for later convenience. It is given by

$$\begin{aligned} G_m(\rho, \rho') &= C_m u_m(\rho_{\max}) v_m(\rho_{\min}) \\ &= C_m \left[u_m(\rho) v_m(\rho') \Theta(\rho - \rho') \right. \\ &\quad \left. + u_m(\rho') v_m(\rho) \Theta(\rho' - \rho) \right], \end{aligned} \quad (\text{S97})$$

where ρ_{\max} (ρ_{\min}) is the maximum (minimum) of ρ and ρ' , and C_m a constant to be determined. To verify Eq. (S96), use $L_m u_m = 0$ and $L_m v_m = 0$ and the definition of L_m to find

$$L_m G_m(\rho, \rho') = 4C_m \kappa_m(\rho) \delta(\rho - \rho'), \quad (\text{S98})$$

where

$$\kappa_m(\rho) = p(\rho) \left[u'_m(\rho) v_m(\rho) - u_m(\rho) v'_m(\rho) \right] \quad (\text{S99})$$

$$= -\frac{4^m \Gamma(\frac{\nu+m+2}{2}) \Gamma(\frac{\nu+m+1}{2})}{\Gamma(\frac{\nu-m+2}{2}) \Gamma(\frac{\nu-m+1}{2})} \quad (\text{S100})$$

is constant and follows from the Wronskian of Legendre's functions [61]. Thus we have to choose $C_m = -1/\kappa_m$ and find

$$C_m = \frac{\Gamma(\frac{\nu-m+2}{2}) \Gamma(\frac{\nu-m+1}{2})}{4^m \Gamma(\frac{\nu+m+2}{2}) \Gamma(\frac{\nu+m+1}{2})} \quad (\text{S101})$$

or

$$C_0 = 1, \quad (\text{S102})$$

$$C_{m \neq 0} = \frac{(-1)^{|m|}}{\prod_{n=0}^{|m|-1} [(n + \frac{1}{2})^2 + \frac{1}{4}(\lambda - 1)]}. \quad (\text{S103})$$

We conclude that the fundamental solution of $\lambda + \Delta_g$ is given by

$$\mathcal{G}_0(z, z', \lambda) = \frac{1}{2\pi} \sum_{m=-\infty}^{\infty} e^{im(\phi - \phi')} G_m(\rho, \rho'). \quad (\text{S104})$$

Indeed, using $\sum_m e^{im(\phi-\phi')} = 2\pi\delta(\phi-\phi')$ and

$$(1-|z|^2)^2\delta^{(2)}(z-z') = \frac{(1-r^2)^2}{r}\delta(r-r')\delta(\phi-\phi') \\ = 4\delta(\rho-\rho')\delta(\phi-\phi') \quad (\text{S105})$$

we verify

$$(\lambda + \Delta_g)\mathcal{G}_0(z, z', \lambda) = \frac{1}{2\pi} \sum_{m=-\infty}^{\infty} e^{im(\phi-\phi')} L_m G_m(\rho, \rho') \\ = -\frac{1}{2\pi} \sum_{m=-\infty}^{\infty} e^{im(\phi-\phi')} 4\delta(\rho-\rho') \\ = -(1-|z|^2)^2\delta^{(2)}(z-z'). \quad (\text{S106})$$

Equation (S104) for the fundamental solution \mathcal{G}_0 allows to easily construct the correction $\delta\mathcal{G}$ such that the total Green function $G = \mathcal{G}_0 - \delta\mathcal{G}$ satisfies Dirichlet boundary conditions: If either $|z| = L$ or $|z'| = L$, then $\rho_{\max} = \frac{1+L^2}{1-L^2}$. Consequently, we choose

$$\delta\mathcal{G}(z, z', \lambda, L) \\ = \frac{1}{2\pi} \sum_{m=-\infty}^{\infty} e^{im(\phi-\phi')} C_m v_m(\rho) v_m(\rho') \frac{u_m(\frac{1+L^2}{1-L^2})}{v_m(\frac{1+L^2}{1-L^2})}. \quad (\text{S107})$$

This is a harmonic function and satisfies $\mathcal{G}_0 = \delta\mathcal{G}$ whenever $|z| = L$ or $|z'| = L$. As an illustrative example consider the central correlation function for $z' = 0$. We have

$$G(z, 0, \lambda, L) = \frac{1}{2\pi} \left[Q_\nu\left(\frac{1+r^2}{1-r^2}\right) - \frac{Q_\nu(\frac{1+L^2}{1-L^2})}{P_\nu(\frac{1+L^2}{1-L^2})} P_\nu\left(\frac{1+r^2}{1-r^2}\right) \right], \quad (\text{S108})$$

clearly vanishing for $r = L$.

The Green function for $L = 1$ can be given in closed form, because it can only depend on the hyperbolic invariant $d(z, z')$. Making the ansatz $\mathcal{G}(z, z', \lambda, 1) = F(y)$ with

$$y = \cosh(2d(z, z')) = 1 + \frac{2|z-z'|^2}{(1-|z|^2)(1-|z'|^2)}, \quad (\text{S109})$$

we find for $z \neq z'$ (or $y > 1$) that

$$0 \stackrel{!}{=} (\lambda + \Delta_g)F(y) \\ = -2\left[(1-y^2)F''(y) - 2yF'(y) - \frac{\lambda}{4}F(y)\right], \quad (\text{S110})$$

which again is Legendre's differential equation. The singular contribution gives the fundamental solution, because

$$Q_\nu(y \rightarrow 1) \sim -\ln\left(\frac{1}{2}\text{arcosh}(y)\right) + \text{const}, \quad (\text{S111})$$

and the regular solution is the harmonic correction to ensure the Dirichlet boundary condition. Hence

$$\mathcal{G}(z, z', \lambda, 1) = \frac{1}{2\pi} \left[Q_\nu(y) - \mathcal{C} \cdot P_\nu(y) \right] \quad (\text{S112})$$

with

$$\mathcal{C} = \lim_{y \rightarrow \infty} \frac{Q_\nu(y)}{P_\nu(y)}. \quad (\text{S113})$$

Importantly, since the fundamental solution does not depend on L , it is *always* given by [55]

$$\mathcal{G}_0(z, z', \lambda) = \frac{1}{2\pi} Q_\nu \left(1 + \frac{2|z-z'|^2}{(1-|z|^2)(1-|z'|^2)} \right). \quad (\text{S114})$$

To compute the constant \mathcal{C} , the parameter λ needs to be restricted to $\lambda \in \mathbb{C} \setminus [1, \infty)$, since the spectrum $k^2 + 1$ of $-\Delta_g$ on the infinite disk is in the interval $[1, \infty)$. For real $\lambda < 1$ this implies $\nu < -1/2$. We expand $P_\nu(y)$ and $Q_\nu(y)$ for large y and arrive at

$$\mathcal{C} = \frac{2^\nu i^{-\nu} \pi^{3/2} \Gamma(-\nu)}{\Gamma(1+\frac{\nu}{2}) \Gamma(\frac{1+\nu}{2})} \left[-\cos\left(\frac{\pi\nu}{2}\right) \frac{\Gamma(1+\frac{\nu}{2})^2}{\Gamma(\frac{1-\nu}{2})^2} \right. \\ \left. + i \sin\left(\frac{\pi\nu}{2}\right) \frac{\Gamma(\frac{1+\nu}{2})^2}{\Gamma(-\frac{\nu}{2})^2} \right]. \quad (\text{S115})$$

S8. CONTINUUM GREEN FUNCTION (SUMMARY)

We summarize the expressions for the Green function $G(z, z', \lambda, L)$ derived in the previous section. We write

$$G(z, z', \lambda, L) = \mathcal{G}_0(z, z', \lambda) - \delta\mathcal{G}(z, z', \lambda, L), \quad (\text{S116})$$

where the first term is given by

$$\mathcal{G}_0(z, z', \lambda) = \frac{1}{2\pi} Q_\nu \left(1 + \frac{2|z-z'|^2}{(1-|z|^2)(1-|z'|^2)} \right) \quad (\text{S117})$$

with $Q_\nu = Q_\nu^{m=0}$ the Legendre function of the second kind and

$$\nu = \frac{1}{2} \left(-1 + i\sqrt{\lambda-1} \right). \quad (\text{S118})$$

The second term reads

$$\delta\mathcal{G}(z, z', \lambda, L) = \frac{1}{2\pi} P_\nu(\rho) P_\nu(\rho') \frac{Q_\nu(\frac{1+L^2}{1-L^2})}{P_\nu(\frac{1+L^2}{1-L^2})} \\ + \frac{1}{\pi} \sum_{m=1}^{\infty} C_m \cos[m(\phi-\phi')] P_\nu^m(\rho) P_\nu^m(\rho') \frac{Q_\nu^m(\frac{1+L^2}{1-L^2})}{P_\nu^m(\frac{1+L^2}{1-L^2})}. \quad (\text{S119})$$

with P_ν^m and Q_ν^m the Legendre function of the first and second kind, hyperbolic invariant

$$\rho = \frac{1+r^2}{1-r^2}, \quad (\text{S120})$$

and

$$C_m = \frac{\Gamma(\frac{\nu-m+2}{2})\Gamma(\frac{\nu-m+1}{2})}{4^m \Gamma(\frac{\nu+m+2}{2})\Gamma(\frac{\nu+m+1}{2})}. \quad (\text{S121})$$

In practice, it is sufficient to limit the sum over m to the first few (typically ten or less) terms. For $L = 1$ we have

$$\delta\mathcal{G}(z, z', \lambda, 1) = \frac{\mathcal{C}}{2\pi} P_\nu \left(1 + \frac{2|z - z'|^2}{(1 - |z|^2)(1 - |z'|^2)} \right) \quad (\text{S122})$$

with $P_\nu = P_\nu^{m=0}$ and

$$\mathcal{C} = \frac{2^\nu \mathrm{i}^{-\nu} \pi^{3/2} \Gamma(-\nu)}{\Gamma(1 + \frac{\nu}{2}) \Gamma(\frac{1+\nu}{2})} \left[-\cos\left(\frac{\pi\nu}{2}\right) \frac{\Gamma(1 + \frac{\nu}{2})^2}{\Gamma(\frac{1-\nu}{2})^2} + \mathrm{i} \sin\left(\frac{\pi\nu}{2}\right) \frac{\Gamma(\frac{1+\nu}{2})^2}{\Gamma(-\frac{\nu}{2})^2} \right]. \quad (\text{S123})$$